Article

Fibular reduction and the evolution of theropod locomotion

https://doi.org/10.1038/s41586-024-08251-w

Received: 24 June 2024

Accepted: 18 October 2024

Published online: 20 November 2024

Check for updates

Armita R. Manafzadeh[1,2,3]✉, Stephen M. Gatesy[4], John A. Nyakatura[5] & Bhart-Anjan S. Bhullar[2,3]

Since Hampé's classic developmental experiments in the mid-twentieth century[1,2], the reduced avian fibula has sparked sustained curiosity[3–6]. The fibula transformed throughout dinosaur evolution from a columnar structure into its splint-like avian form, a change long thought to be of little biomechanical consequence[3,6]. Here we integrated comparative three-dimensional kinematic analyses with transitional morphologies from the fossil record to refute this assumption and show that the reduced fibula serves a crucial function in enabling extreme knee long-axis rotation (LAR). Extreme LAR is fundamental to avian locomotion and is regularly exploited by living birds to execute complex terrestrial manoeuvres[7]. We infer that the evolution of this capacity was preceded by restriction of the knee to hinge-like motion in early theropod dinosaurs, driven by the origin of a mid-shank articulation[8] that precluded ancestral patterns of tibiofibular motion. Freeing of the fibula from the ankle joint later enabled mobilization of this initially static articulation and, in doing so, established a novel pattern of tibiofibular kinematics essential to the extreme levels of LAR retained by modern birds. Fibular reduction thus ushered in a transition to LAR-dominated three-dimensional limb control, profoundly altering the course of theropod locomotor evolution.

From diving ducks to hovering hummingbirds, the more than 10,000 species of extant birds exhibit myriad variations on a recognizable avian theme. The basic bauplan uniting this diversity originated during the Mesozoic Era, when it was slowly assembled through piecewise modification of the ancestral reptilian condition[9]. Perhaps most famously, the forelimb was elaborated into a feathered and aerodynamic wing[10] — essential in the evolution of powered flight[11] — and the snout was elongated into a pointed and dexterous beak[12] — a key component of the avian kinetic apparatus[13]. In concert with the acquisition of these morphofunctional innovations, the hindlimb also underwent a dramatic transformation. Whereas the ancestral reptilian crus (shank) comprised a robust, columnar tibia and fibula extending from the knee to the ankle, the fossil record of theropod dinosaurs documents a sequential and severe reduction of the fibula on the line to birds. Modern birds consequently possess gracile, splint-like fibulas radically different from those of lepidosaurs and crocodilians (Fig. 1a,b). Such crural disparity has long perplexed developmental biologists, who have sought to elucidate its underpinnings by inducing atavistic morphology in avian embryos[1–6]. Despite an enduring fascination with fibular reduction, however, this transformation is widely assumed to have no direct adaptive value[3,6], and its biomechanical implications remain largely unexplored.

Skeletal motion in the reptilian crus

To illuminate the functional impact of fibular reduction, we visualized and measured skeletal motion in the hindlimbs of three species of living reptiles: a lepidosaur, the green iguana (*Iguana iguana*); a crocodilian, the American alligator (*Alligator mississippiensis*); and a bird, the helmeted guineafowl (*Numida meleagris*), using X-ray Reconstruction of Moving Morphology (XROMM)[14,15]. As predicted by the reptilian 'crural mechanism' hypothesis[16], both the iguana and the alligator demonstrate anteroposterior and proximodistal skewing of the fibula relative to the tibia (Fig. 2a,b, Extended Data Fig. 1 and Supplementary Videos 1 and 2). However, we found that the avian crus displays a fundamentally different kinematic pattern: the fibula rolls axially, pivoting about its unique midshaft articulation with the tibiotarsus (as predicted by ref. 17; Figs. 1b and 2c, Extended Data Figs. 1 and 2 and Supplementary Video 3). Evidence from our XROMM animations (Extended Data Fig. 3) suggests that this rolling motion is most pronounced during sequences of knee LAR (sensu ref. 18; Fig. 2d,e). Although avian knee joints were long thought to operate as simple hinges[19], recent analyses have indicated that the tibiotarsus can spin axially by more than 100° relative to the femur[7,20].

LAR at the archosaur knee

Motivated by the dissimilarity of intracrural kinematics that we observed in living animals, we then undertook a more comprehensive analysis of cadaveric individuals to characterize passive differences in tibiofibular mobility. XROMM investigation of cadaveric archosaurs (alligators and birds; following refs. 21,22; Extended Data Fig. 4) enabled us to uncover the skeletal basis of extreme avian knee LAR potential, of

[1]Yale Institute for Biospheric Studies, Yale University, New Haven, CT, USA. [2]Department of Earth and Planetary Sciences, Yale University, New Haven, CT, USA. [3]Yale Peabody Museum of Natural History, New Haven, CT, USA. [4]Department of Ecology, Evolution, and Organismal Biology, Brown University, Providence, RI, USA. [5]Institut für Biologie, Humboldt Universität zu Berlin, Berlin, Germany. ✉e-mail: armita.manafzadeh@yale.edu

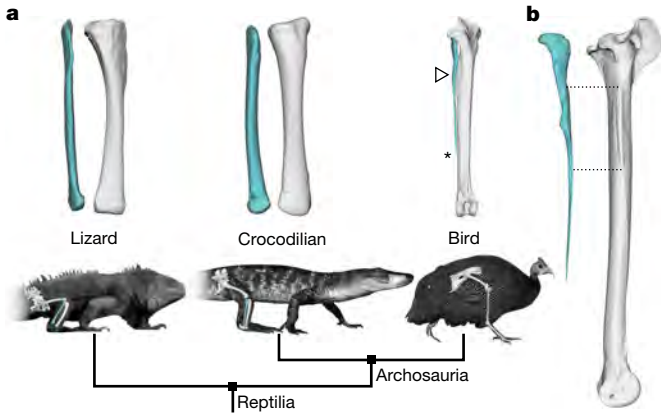

Fig. 1 | Crural architecture of extant reptiles. a, The hindlimbs of extant lizards (represented by *I. iguana*) and crocodilians (represented by *A. mississippiensis*) retain the ancestral reptilian condition of robust, columnar tibias and fibulas. By contrast, the avian crus (represented by *N. meleagris*) features a highly reduced fibula with a unique midshaft intracrural articulation (indicated by the arrowhead) but no distal connection to the ankle joint. The end of the fibula is indicated by an asterisk. The right crura are in anterior view. **b**, In birds, the fibula and tibiotarsus articulate at the site of a lateral bony expansion of the tibiotarsus: the fibular crest. The right fibula and tibiotarsus are in lateral view. The proximodistal extent of the intracrural articulation is indicated with dashed lines. The fibula is in cyan throughout.

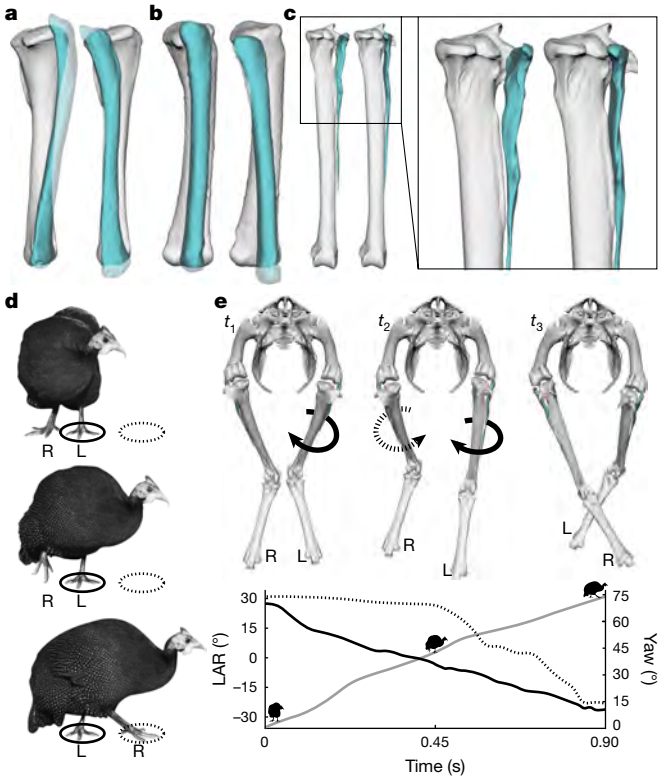

Fig. 2 | Intracrural motion in living reptiles. a, In the iguanan crus, the fibula undergoes skewing relative to the tibia (in right lateral view). **b**, Intracrural motion in the alligator is much like that in the iguana (in right lateral view). **c**, In the bird, the fibula displays a fundamentally different kinematic pattern, hinging about its midshaft articulation with the tibiotarsus to roll axially (in posterior view). This rolling motion is most prominent during sequences of knee LAR. Birds exploit extreme knee LAR to manoeuvre. **d**, Standard camera images of a helmeted guineafowl making a sharp left turn. The left foot (L) remains planted on the ground as the body reorients. The right foot (R) crosses over the left to initiate a step on the new heading. **e**, XROMM-derived avian hindlimb skeletons at three time points (t_1–t_3) during a sharp left turn, shown relative to a fixed pelvic reference frame in anterior view (top) and corresponding kinematic curves (bottom). A yaw of 73° (grey solid line) is accompanied by 54° of relatively steady internal left knee LAR (black solid line (bottom) and black curved arrows (top)), which spins the body relative to the planted left foot (t_1–t_3). Once lifted (t_2–t_3), the right knee undergoes rapid internal knee LAR of 55° (black dashed line (bottom) and curved dashed arrow (top)) to reorient the foot for the next step. Fibulas are in cyan throughout.

which the reduced fibula is an essential component. Through articular raycasting analysis[23], we found that the archosaur knee involves three homologous relationships: (1) medial femoral condyle–medial proximal tibia, (2) lateral femoral condyle–lateral proximal tibia, and (3) femoral fibular trochlea–fibular head (femoral terminology follows ref. 24; Fig. 3, Extended Data Fig. 5 and Supplementary Videos 4 and 5). During LAR in both alligators and birds, the medial femoral condyle traces an arc across the proximal medial tibia or tibiotarsus while the lateral femoral condyle traces an arc along the proximal lateral tibia or tibiotarsus. Extreme avian LAR is facilitated by the flattened, reniform morphology of the proximal medial tibiotarsal surface and the canted, conical morphology of the proximal lateral tibiotarsal surface, which create an extended arc length traversed by the femur (Fig. 3h). In both taxa, intracrural motion allows the fibular head to remain engaged with the femoral trochlea throughout this dynamic tibiofemoral interaction. LAR in the alligator is limited because the fibula contributes to both the knee and the ankle joints, necessitating a kinematic compromise between femoral and pedal motion. Similar constraints presumably apply to iguanas and other reptiles with comparable crural architecture. By contrast, the reduced avian fibula is detached from the ankle, permitting it greater freedom to maintain articulation with the femur throughout LAR. Over 85° of hinge-like mobility at the midshaft intracrural articulation allows the avian fibular head to remain nestled tightly within the femoral trochlea while the tibiotarsus undergoes extreme axial rotation (Extended Data Fig. 4).

Evolution of extreme LAR

With the understanding gained from living animals that extreme knee LAR relies on both proximal tibial or tibiotarsal geometry and fibular reduction, we turned to the fossil record to reconstruct the evolutionary assembly of this functional capacity. We collated a representative sample of extinct reptiles on the line to birds – the dinosauromorph *Marasuchus lilloensis*, the tetanuran *Allosaurus fragilis*, the dromaeosaur *Deinonychus antirrhopus*, the probable basal avialan *Rahonavis ostromi* and the ornithuran *Ichthyornis dispar* – and applied our knowledge of articulation in extant archosaurs (Fig. 3) to delineate homologous osteological surfaces for each taxon (Fig. 4 and Supplementary Fig. 1).

By tracking evolutionary transformations in knee joint articular morphology, we found that the elaborated tibiotarsal arc present in modern birds arose late in theropod evolution and was not the culmination of a unidirectional trend. Rather, an initial transformation away from the primitive reptilian condition of moderate tibial articular curvature[25–27] (maintained by *Alligator* and *Marasuchus*), yielded straighter, more anteroposteriorly directed surfaces in *Allosaurus* and other non-maniraptoran tetanurans[28–30] (of various body sizes; Extended Data Fig. 6 and Supplementary Information). This straightening was then followed by a gradual return to tibial surface curvature, exemplified by *Deinonychus*, *Rahonavis* and other non-ornithothoracine maniraptorans[31–33], ultimately resulting in the extended arc present in ornithothoracines including *Ichthyornis* and modern birds[34–36] (Extended Data Fig. 6 and Supplementary Information).

Viewing these transformations in tibial or tibiotarsal articular surface geometry within the context of concurrent modifications to hindlimb architecture (Fig. 4) exposes an initial trend in the theropod knee not towards extreme mobility, but rather towards hinge-like

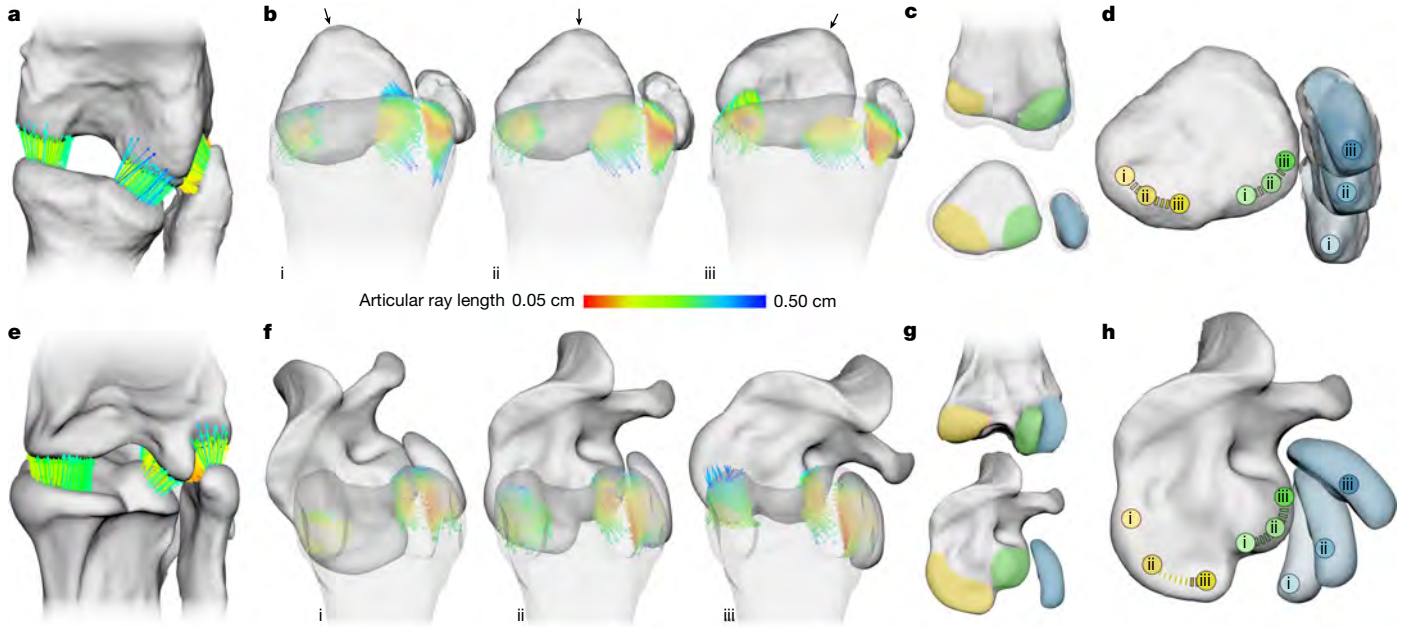

Fig. 3 | Articular raycasting analysis of archosaurian knee LAR. a, Casting rays from the crus to the femur enables evaluation of articular surface interactions throughout alligator knee LAR. The right knee is in posterior view. **b**, Motion of the right crural bones and corresponding articular rays at internally rotated (i), intermediate (ii) and externally rotated (iii) knee poses relative to a fixed femoral reference frame. A proximal view of the right crus through a fixed distal femur (semi-transparent) is shown. The arrows follow the rotation of the anterior tibia. **c**, Delineation of interacting articular regions on osteological surfaces: medial femoral condyle–medial proximal tibia (yellow), lateral femoral condyle–lateral proximal tibia (green) and femoral fibular trochlea–fibular head (blue). **d**, The femoral condyles trace arc-like paths across the proximal tibial surfaces, while the fibula moves relative to the tibia, throughout knee LAR. The motion is represented relative to a fixed tibial reference frame. The Roman numerals denote the positions of a fixed point on each femoral condyle and correspond to the three configurations shown in panel **b**. **e**–**h**, As for panels **a**–**d**, respectively, but for the bird knee. Articular rays in panels **a**,**b**,**e**,**f** are coloured by their lengths as indicated in the legend.

restriction. The ancestral reptilian hindlimb had substantial potential for intracrural and intertarsal motion[37,38]. Using homologous intracrural kinematics broadly similar to the 'skewing' of the living iguana and alligator (Fig. 2a,b) allowed early reptiles to achieve moderate levels of knee LAR during both steady and manoeuvring locomotion. By contrast, non-dinosaurian dinosauromorphs such as *Marasuchus* modified the ancestral tarsus and metatarsus, decreasing ankle mobility[39] and therefore the distal independence of the tibia and fibula. Reduced intracrural mobility forced the tibia and fibula to move largely in unison, limiting the extent to which the tibia could spin without the fibular head either colliding with or disengaging from the femoral trochlea. In tetanuran theropods such as *Allosaurus*, not only were the tarsus and ankle joint further rigidified but the tibia also possessed a novel, lateral expansion of a midshaft bone called the 'fibular crest'. This structure more firmly anchored the proximal fibula to the tibia and severely restricted intracrural mobility[8,17]. Coupled with the presence of more linear crural articular surfaces, such immobility rendered appreciable LAR all but impossible, constraining the tetanuran knee to hinge-like motion.

Perhaps counterintuitively, we found that this rigidification phase of theropod hindlimb evolution was a necessary precursor for the origin of extreme knee LAR. The tarsal and crural structure of early paravians such as *Deinonychus* was much like that of non-paravian theropods, albeit with a more slender fibula. The return towards increased proximal tibial curvature probably facilitated a modest increase in knee LAR among these taxa. However, it was not until avialans tapered the fibula to the point of flexibility and freed it from its distal connection to the ankle that LAR capacity could markedly increase. We propose that fibular reduction enabled mobilization of the articulation between the tibia and the fibula at the site of the theropodan fibular crest, leading to the reacquisition of intracrural mobility. Co-option of the previously stabilizing midshaft articulation led the fibula to take on a new, rolling kinematic pattern resembling that of the living bird (Fig. 2c). Ornithothoracines then built from this fundamentally new mechanism for knee LAR by further elaborating the proximal tibiotarsal arc. As a result, these animals were able to achieve, for the first time, the extreme levels of LAR that we see retained by birds today.

Of course, theropod evolution was not an orthogenetic march towards the avian condition. Current phylogenetic hypotheses[29,40,41] depict the dinosaur tree as rife with convergence, featuring at least three independent reductions of the fibula (and concomitant transformations of knee joint surfaces) following the theropod origin of the fibular crest. The form–function relationships that we have uncovered here introduce a new lens through which to reassess the full spectrum of theropod hindlimb diversity. Adopting this perspective, we hypothesize that co-option of the tibiofibular articulation, reacquisition of intracrural mobility and enhancement of knee LAR took place not only among avialans but also among alvarezsaurids[42,43] and oviraptorosaurs[44,45] (Supplementary Information). The implications of independent fibular reduction in pterosaurs remain to be explored, complicated by controversy surrounding basic aspects of pterosaurian locomotion. On the basis of the presence of a reduced fibula, a midshaft intracrural articulation and arced proximal tibiotarsal geometry in at least some pterodactyloids[46], we tentatively suggest that these taxa may also have evolved an avialan-style mechanism for knee LAR. Although some ornithischian dinosaurs also display slender fibulas grossly similar to those of non-avialan paravians, in the absence of a fibular crest, it remains to be determined what the functional implications of such morphology might be, if any.

Functional impact of fibular reduction

It has long been assumed that a reduced fibula is merely the developmental byproduct of adaptive changes to other hindlimb elements.

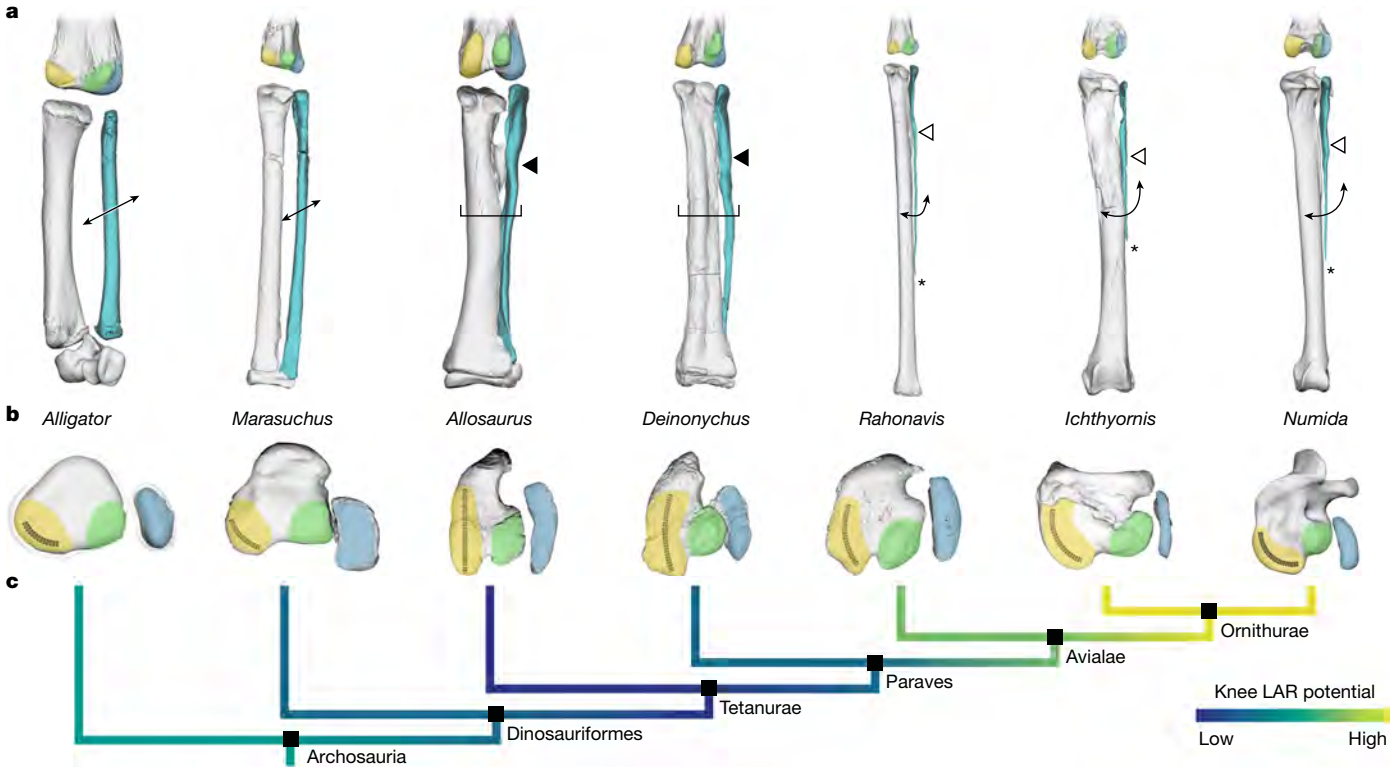

Fig. 4 | The evolutionary origin of extreme knee LAR in birds. a, Differences in the distal femoral, crural and proximal tarsal skeletal architecture (posterior view of the right limbs) suggest transformations in intracrural kinematics. The fibula is in cyan; the femoral colours reflect articular surface homology as in Fig. 3. The slanted arrows indicate skewing intracrural kinematics; the brackets indicate limited intracrural motion; the curved arrows indicate axial rolling of the fibula about the intracrural articulation; and the relative size of arrows reflects the degree of intracrural mobility. The black arrowheads indicate the presence of a fibular crest on the tibia; the white arrowheads indicate mobility at the midshaft intracrural articulation. The asterisks indicate the end of the reduced fibula. **b**, Crural articular geometry (in proximal view) demonstrates changes in curvature of the proximal medial tibial or tibiotarsal surface (in yellow), resulting in differences in the capacity of the medial femoral condyle to travel along an arc-like path, summarized by actual (bold) and inferred potential trajectories marked on each surface, following Fig. 3. The colours reflect articular surface homology as in Fig. 3. Medial femoral condyle paths for *Alligator* and *Numida* reproduce observed cadaveric data from Fig. 3. **c**, Inferred evolutionary trends in knee LAR potential among archosaurs, based on the morphological changes in panels **a**,**b** and the results from extant animals depicted in Figs. 2 and 3. The phylogenetic placements follow refs. 29,40,41.

Here we reject this premise and propose, much to the contrary, that fibular reduction had a substantial functional role in theropod locomotor evolution. Early tetanuran theropods, with their hinge-like knees and ankles, probably relied on hip mobility in conjunction with tail dynamics to navigate terrestrial environments[8]. However, forelimb enlargement, tail reduction, anterior centre of mass displacement and the transition to a more crouched posture along the bird-line rendered this strategy progressively less effective in modulating pedal placement and orientation[7,47,48], even as the knee gained some LAR potential among early paravians (Fig. 4).

Fibular reduction and co-option of the midshaft tibiofibular articulation unlocked a novel, LAR-dominated solution for three-dimensional limb control, vastly expanding the avialan – and ultimately avian – locomotor repertoire. Our XROMM analyses captured birds in the laboratory exploiting extreme knee LAR to nimbly turn, manoeuvre and evade obstacles. We suspect that among the avialan radiation, this capacity also had (and continues to have) an unappreciated role in navigating complex arboreal substrates and in foot-propelled diving, as well as in crucial non-locomotor behaviours, such as preening, courtship and prey capture.

In avian embryos, fibular reduction appears to involve migration of the fibulare, which becomes closely appressed to the distal end of the fibula and acts as a 'surrogate epiphysis' before later separating and disrupting the paracrine feedback loop underlying distal fibular growth[3]. The fibula–fibulare proximity necessary for such 'surrogation' has been suggested to be an ornithodiran apomorphy[3], making it probable that embryonic separation of the fibulare and disruption of the distal fibular signalling regime also led to fibular reduction in alvarezsaurids, oviraptorosaurs and pterosaurs. We therefore conclude that the adaptive benefits of fibular reduction drove convergent transformation of crural development at least three, possibly four, times in the known history of reptiles. Such intricate interplay between functional and developmental mechanisms is undoubtedly commonplace in the origin of morphological innovations[5,49], underscoring the need for further integration of whole-organism biomechanics and evolutionary developmental biology[50].

Online content

Any methods, additional references, Nature Portfolio reporting summaries, source data, extended data, supplementary information, acknowledgements, peer review information; details of author contributions and competing interests; and statements of data and code availability are available at https://doi.org/10.1038/s41586-024-08251-w.

1. Hampé, A. Le développement du péroné dans les experiences sur la régulation des déficiences et des excédents dans la patte du Poulet. *Development* **6**, 215–222 (1958).
2. Wolff, E. & Hampé, A. Sur la régulation de la patte du poulet après résection d'un segment intermédiaire du bourgeon de membre. *Compt. Rend. Soc. Biol.* **148**, 154–156 (1954).
3. Botelho, J. F. et al. Molecular development of fibular reduction in birds and its evolution from dinosaurs. *Evolution* **70**, 543–554 (2016).
4. Goff, D. J. & Tabin, C. J. Analysis of Hoxd-13 and Hoxd-11 misexpression in chick limb buds reveals that Hox genes affect both bone condensation and growth. *Development* **124**, 627–636 (1997).

5. Müller, G. B. & Streicher, J. Ontogeny of the syndesmosis tibiofibularis and the evolution of the bird hindlimb: a caenogenetic feature triggers phenotypic novelty. *Anat. Embryol.* **179**, 327–339 (1989).
6. Streicher, J. & Müller, G. B. Natural and experimental reduction of the avian fibula: developmental thresholds and evolutionary constraint. *J. Morphol.* **214**, 269–285 (1992).
7. Kambic, R. E., Roberts, T. J. & Gatesy, S. M. Long-axis rotation: a missing degree of freedom in avian bipedal locomotion. *J. Exp. Biol.* **217**, 2770–2782 (2014).
8. Farlow, J. O., Gatesy, S. M., Holtz, T. R. Jr, Hutchinson, J. R. & Robinson, J. M. Theropod locomotion. *Am. Zool.* **40**, 640–663 (2000).
9. Brusatte, S. L., O'Connor, J. K. & Jarvis, E. D. The origin and diversification of birds. *Curr. Biol.* **25**, R888–R898 (2015).
10. Zelenitsky, D. K. et al. Feathered non-avian dinosaurs from North America provide insight into wing origins. *Science* **338**, 510–514 (2012).
11. Dial, K. P. Evolution of avian locomotion: correlates of flight style, locomotor modules, nesting biology, body size, development, and the origin of flapping flight. *The Auk* **120**, 941–952 (2003).
12. Bhullar, B. A. S. et al. Birds have paedomorphic dinosaur skulls. *Nature* **487**, 223–226 (2012).
13. Bout, R. G. & Zweers, G. A. The role of cranial kinesis in birds. *Comp. Biochem. Physiol. A Mol. Integr. Physiol.* **131**, 197–205 (2001).
14. Brainerd, E. L. et al. X-ray reconstruction of moving morphology (XROMM): precision, accuracy and applications in comparative biomechanics research. *J. Exp. Zool. A Ecol. Genet. Physiol.* **313**, 262–279 (2010).
15. Gatesy, S. M., Baier, D. B., Jenkins, F. A. & Dial, K. P. Scientific rotoscoping: a morphology-based method of 3-D motion analysis and visualization. *J. Exp. Zool. A Ecol. Genet. Physiol.* **313**, 244–261 (2010).
16. Landsmeer, J. M. Functional morphology of the hindlimb in some lacertilia. *Eur. J. Morphol.* **28**, 3–34 (1990).
17. Fuss, F. K. Tibiofibular junction of the South African ostrich (*Struthio camelus australis*). *J. Morphol.* **227**, 213–226 (1996).
18. Gatesy, S. M. et al. A proposed standard for quantifying 3-D hindlimb joint poses in living and extinct archosaurs. *J. Anat.* **241**, 101–118 (2022).
19. Hertel, F. & Campbell, K. E. Jr The antitrochanter of birds: form and function in balance. *The Auk* **124**, 789–805 (2007).
20. Manafzadeh, A. R., Kambic, R. E. & Gatesy, S. M. A new role for joint mobility in reconstructing vertebrate locomotor evolution. *Proc. Natl Acad. Sci. USA* **118**, e2023513118 (2021).
21. Manafzadeh, A. R. A practical guide to measuring ex vivo joint mobility using XROMM. *Integr. Org. Biol.* **2**, obaa041 (2020).
22. Manafzadeh, A. R. Joint mobility as a bridge between form and function. *J. Exp. Biol.* **226**, jeb245042 (2023).
23. Manafzadeh, A. R., Gatesy, S. M. & Bhullar, B. A. S. Articular surface interactions distinguish dinosaurian locomotor joint poses. *Nat. Commun.* **15**, 854 (2024).
24. Baumel, J. J., King, A. S., Lucas, A. M., Breazile, J. E. & Evans, H. E. (eds) *Nomina Anatomica Avium: an Annotated Anatomical Aictionary of Birds* (1981).
25. Haines, R. W. The tetrapod knee joint. *J. Anat.* **76**, 270–301 (1942).
26. Holmes, R. B. The hind limb of *Captorhinus aguti* and the step cycle of basal amniotes. *Can. J. Earth Sci.* **40**, 515–526 (2003).
27. Vaughn, P. P. The Permian reptile *Araeoscelis* restudied. *Bull. Mus. Comp. Zool.* **113**, 303–467 (1955).
28. Allain, R., Vullo, R., Le Loeuff, J. & Tournepiche, J. F. European ornithomimosaurs (Dinosauria, Theropoda): an undetected record. *Geol. Acta* **12**, 127–135 (2014).
29. Rauhut, O. W. & Pol, D. Probable basal allosauroid from the early Middle Jurassic Cañadón Asfalto Formation of Argentina highlights phylogenetic uncertainty in tetanuran theropod dinosaurs. *Sci. Rep.* **9**, 18826 (2019).
30. White, M. A. et al. New *Australovenator* hind limb elements pertaining to the holotype reveal the most complete neovenatorid leg. *PLoS ONE* **8**, e68649 (2013).
31. Novas, F. E., Egli, F. B., Agnolin, F. L., Gianechini, F. A. & Cerda, I. Postcranial osteology of a new specimen of *Buitreraptor gonzalezorum* (Theropoda, Unenlagiidae). *Cretaceous Res.* **83**, 127–167 (2018).
32. Xu, X., Norell, M. A., Wang, X. L., Makovicky, P. J. & Wu, X. C. A basal troodontid from the Early Cretaceous of China. *Nature* **415**, 780–784 (2002).
33. Zanno, L. E. Osteology of *Falcarius utahensis* (Dinosauria: Theropoda): characterizing the anatomy of basal therizinosaurs. *Zool. J. Linn. Soc.* **158**, 196–230 (2010).
34. Forster, C. A., Chiappe, L. M., Krause, D. W. & Sampson, S. D. The first Cretaceous bird from Madagascar. *Nature* **382**, 532–534 (1996).
35. Kurochkin, E. N. & Molnar, R. E. New material of enantiornithine birds from the Early Cretaceous of Australia. *Alcheringa* **21**, 291–297 (1997).
36. Zinoviev, A. V. Notes on the hindlimb myology and syndesmology of the Mesozoic toothed bird *Hesperornis regalis* (Aves: Hesperornithiformes). *J. Syst. Paleontol.* **9**, 65–84 (2011).
37. Rewcastle, S. C. Fundamental adaptations in the lacertilian hind limb: a partial analysis of the sprawling limb posture and gait. *Copeia* **2**, 476–487 (1983).
38. Schaeffer, B. The morphological and functional evolution of the tarsus in amphibians and reptiles. *Bull. Am. Mus. Nat. Hist.* **78**, 6 (1941).
39. Turner, M. L. & Gatesy, S. M. Inner workings of the alligator ankle reveal the mechanistic origins of archosaur locomotor diversity. *J. Anat.* **242**, 592–606 (2023).
40. Turner, A. H., Makovicky, P. J. & Norell, M. A. A review of dromaeosaurid systematics and paravian phylogeny. *Bull. Am. Mus. Nat. Hist.* **2012**, 1–206 (2012).
41. Xu, X. et al. Two Early Cretaceous fossils document transitional stages in alvarezsaurian dinosaur evolution. *Curr. Biol.* **28**, 2853–2860 (2018).
42. Novas, F. E. Anatomy of *Patagonykus puertai* (Theropoda, Avialae, Alvarezsauridae), from the late Cretaceous of Patagonia. *J. Vertebr. Paleontol.* **17**, 137–166 (1997).
43. Altangerel, P., Norell, M. A., Chiappe, L. M. & Clark, J. M. Flightless bird from the Cretaceous of Mongolia. *Nature* **362**, 623–626 (1993).
44. Funston, G. F., Currie, P. J., Ryan, M. J. & Dong, Z. M. Birdlike growth and mixed-age flocks in avimimids (Theropoda, Oviraptorosauria). *Sci. Rep.* **9**, 18816 (2019).
45. Currie, P. J., Funston, G. F. & Osmólska, H. New specimens of the crested theropod dinosaur *Elmisaurus rarus* from Mongolia. *Acta Palaeontol. Pol.* **61**, 143–157 (2015).
46. Galton, P. M. Avian-like tibiotarsi of pterodactyloids (Reptilia: Pterosauria) from the Upper Jurassic of East Africa. *Paläontologische Zeitschrift* **54**, 331–342 (1980).
47. Gatesy, S. M. Caudofemoral musculature and the evolution of theropod locomotion. *Paleobiology* **16**, 170–186 (1990).
48. Allen, V., Bates, K. T., Li, Z. & Hutchinson, J. R. Linking the evolution of body shape and locomotor biomechanics in bird-line archosaurs. *Nature* **497**, 104–107 (2013).
49. Erwin, D. H. Novelty and innovation in the history of life. *Curr. Biol.* **25**, R930–R940 (2015).
50. Hernández, L. P., Barresi, M. J. & Devoto, S. H. Functional morphology and developmental biology of zebrafish: reciprocal illumination from an unlikely couple. *Integr. Comp. Biol.* **42**, 222–231 (2002).

Methods

In vivo motion analysis

All procedures involving live animals were approved by the Brown University Institutional Animal Care and Use Committee or the responsible authorities in Thuringia, Germany (Thüringer Landesamt für Verbraucher-und Umweltschutz). Experiments were neither blinded nor randomized.

Hindlimb skeletal motion for the helmeted guineafowl (*N. meleagris*, hereafter 'guineafowl'), the American alligator (*A. mississippiensis*, hereafter 'alligator') and the green iguana (*I. iguana*, hereafter 'iguana') was visualized using a combination of marker-based XROMM[14] and scientific rotoscoping[15].

To minimize live animal use, we reanalysed subsets of existing datasets of guineafowl (adult, female) and alligator (juvenile, female) hindlimb skeletal motion that were previously visualized using marker-based XROMM[7,51], with extended details of surgical methodology, X-ray technique and analysis included therein. In brief, three to five radiopaque conical markers made from carbide steel rods were surgically implanted in the guineafowl pelvis, femur, tibiotarsus and tarsometatarsus, and the alligator pelvis, femur and tibia (as well as other skeletal elements not analysed here). Two markers were also implanted in the alligator fibula, facilitating scientific rotoscoping (see below). Animals were imaged while walking on motorized treadmills (alligator) and manoeuvring in acrylic enclosures (guineafowl) in the W. M. Keck Foundation XROMM Facility at Brown University. Computed tomography (CT) or micro-CT-derived mesh models of each skeletal element were cleaned using Geomagic Wrap 2017 (3D Systems).

Archosaur X-ray videos were calibrated, and radiopaque markers were tracked using XMALab[52] (v2.1.0; see Code availability). Unfiltered rigid body transformations were used to animate the guineafowl pelvis, femur, tibiotarsus and tarsometatarsus and the alligator tibia bone models in Maya 2020–2025 (Autodesk). These marker-based animations were then augmented with fibular motion through scientific rotoscoping in Maya. For the guineafowl, mesh models of the fibula were registered to bone shadows in both X-ray video views[15]. For the alligator, a 'hybrid animation' approach[53] was used in which a base animation of the fibula based on the two implanted markers was refined through registration to bone shadows.

We also reanalysed a subset of an existing dataset of iguana (adult, female) hindlimb motion that was previously visualized by ref. 54, with extended details of X-ray technique and analysis included therein. In brief, one iguana walking along a trackway was imaged at the X-ray facility of the Institut für Zoologie und Evolutionsforschung at Friedrich Schiller University. X-ray videos were calibrated using the MATLAB calibration routine available at xromm.org. For this study, CT-derived mesh models of the pelvis, femur, tibia and fibula were independently registered to bone shadows in both X-ray video views in Maya[15].

Geomagic Wrap was used to fit geometric primitives to femoral, tibial or tibiotarsal and fibular articular surfaces for each individual (following ref. 18). The mesh models and geometric primitives were imported into Maya to create standardized coordinate systems and reference poses following the archosaur coordinate system standards developed by ref. 18, here also applied to *Iguana*. The work in ref. 18 did not outline standards for the creation of separate tibial or tibiotarsal and fibular anatomical coordinate systems (ACSs), instead opting to simplify the crus as a rigid unit to facilitate holistic comparison of knee motion among archosaurs. Given the inadequacy of this simplification for the focus of the present study, here we established a fibular convention following their basic principles. The proximal ACS for each tibia or tibiotarsus ('kneeM' sensu ref. 18) was shifted to the centre of the tibial or tibiotarsal proximal articular region, and was also duplicated and translated to the centre of the corresponding fibular head. This fibular ACS was then rotated about its *x* axis to orient its *y* axis parallel to the major axis of the fibular head. To account for intraspecific differences in tibial or tibiotarsal torsion, proximal tibial and tibiotarsal ACSs were rotated about their *x* axes to maximize proximal crural alignment and comparability within the articular context of this study.

Relative bone motion was calculated from these coordinate systems using a custom Maya embedded language script, oRelFast.mel (see Code availability). This script builds from the existing 'Output Relative Motion' tools available in the XROMM Maya Tools package (see Code availability) to more quickly calculate rotations and translations using node-based matrix calculations.

Cadaveric motion analysis

Potential motion of the femur, tibia or tibiotarsus, and fibula at the knee joints of cadaveric guineafowl and alligators was determined following the ex vivo XROMM protocol previously outlined[21]. Experiments were neither blinded nor randomized. Two intact, fresh-frozen guineafowl (adult, female) cadavers and two intact, fresh-frozen alligator (juvenile, female) cadavers were obtained from colleagues for a previous comparative analysis of archosaur hindlimb mobility[20], with extended details of X-ray technique and analysis included therein. In brief, three to five radiopaque zirconium oxide ball bearings were implanted into hand-drilled holes in one femur, tibiotarsus and fibula of each guineafowl; one femur, tibia and fibula of one alligator; and both femora, tibias and fibulas of the other alligator. All ball bearings were affixed with cyanoacrylate adhesive. Additional skeletal elements were also marked but are not included in the analysis here. Damage to soft tissues was minimized using blunt dissection techniques; all incisions were sutured after marker implantation. Each marked hindlimb was imaged in the W. M. Keck Foundation XROMM Facility at Brown University while being manipulated using one or two 1.0-m wooden dowel rods loosely connected to the hindlimb. Of the guineafowl X-ray data, 10,800 frames were analysed; in 77 of these frames, fibular markers were insufficiently visible to facilitate reliable tracking and these frames were excluded from analysis. Because the alligator fibula reaches the ankle and pedal position therefore influences intracrural kinematics, 19,800 frames of the alligator X-ray data were analysed to ensure inclusion of additional modes of cadaveric manipulation and more complete coverage of mobility; in 11 of these frames, the fibula was out of view and these frames were excluded from analysis.

CT and micro-CT scanning, mesh model creation, geometric primitive fitting, coordinate system creation, video calibration and marker tracking were conducted as described for live individuals. Unfiltered rigid body transformations were calculated using XMALab and used to animate meshes in Maya, where relative bone motion was calculated using oRelFast.mel as above. For the alligator, meshes were created including cartilage to facilitate articular raycasting analysis (see below).

To identify homologous interactions among knee joint articular surfaces, we followed the articular raycasting methodology previously described[23]. In brief, meshes for the femur, tibia/tibiotarsus and fibula for one guineafowl individual and one alligator individual were imported into Maya. Cartilage was included in the alligator meshes to attain the most informative evaluation of in vivo articular relationships; bone meshes were used for the guineafowl because avian knee articular cartilage is thin and does not appreciably change functional articular shape. Functional articular surfaces were estimated based on anatomy and were delineated on the distal femur and proximal tibia or tibiotarsus and fibula for both taxa. Rays of infinite length were then cast from the crural articular surfaces along their vertex normals, and all rays that successfully hit the femur were coloured by their resulting lengths. The results of this preliminary raycast were used to further refine the selection of articular surfaces, and the raycasting process was then repeated. Osteological articular surfaces were delineated for the alligator by identifying the regions of bone overlain by cartilaginous articular surfaces.

Fossil morphology

Three-dimensional meshes of skeletal elements for a sample of extinct reptiles were assembled for comparative anatomical analysis from a combination of existing models and new models created from micro-CT scans of fossils or high-resolution research casts. All new micro-CT scans were conducted at Yale University (Nikon Xtek H 225 ST microCT, Nikon Metrology), and the resulting data were processed using the 'surface determination' and 'convert to mesh' functions in VGStudio MAX 3.4 to create three-dimensional mesh models in OBJ format. Osteological articular surfaces were delineated on each mesh based on changes in surface texture and curvature, and coloured by inferred region homology based on the results of articular raycasting for the guineafowl and alligator (see above).

Meshes of the right femur, right tibia and right fibula of *M. lilloensis* (PVL 3870/3871) were provided by J. Hutchinson and originally published[18] (the details of mesh construction are included in the paper). Existing mirrored left femoral, mirrored left tibial and mirrored left fibular meshes for *A. fragilis* (YPM 4944) originally created by ref. 55 and deposited at the Yale Peabody Museum were supplemented with new meshes created for the mirrored left astragalus (original) and right calcaneum (cast) of the same specimen (175 kV, 68 mA, 1-s exposure and 2,000 projections); all meshes have now been deposited in Morphosource. The *Allosaurus* tibia was taphonomically anteroposteriorly bowed and therefore retrodeformed to straighten the shaft, using the right tibia of YPM 4944 as a reference, with lattice deformers in Maya. Meshes for the right femur and right crus of *D. antirrhopus* (for femur, YPM 53258 (MCZ 4371); for crus, YPM 53258 (AMNH 3015)) were created from micro-CT scans (182 kV, 130 µA, 1-s exposure and 800 projections) of high-resolution casts housed in the Yale Peabody Museum and have been deposited in Morphosource. The *Deinonychus* crus was taphonomically mediolaterally bowed and therefore retrodeformed to straighten the tibial and fibular shafts, using the YPM cast of MCZ 4371 (YPM 53258) as a reference, with lattice deformers in Maya. In all cases, retrodeformation only served to straighten bone shafts and did not influence the morphology of articular surfaces; images of the original, unretrodeformed meshes are provided as Supplementary Fig. 1. Meshes for the right femur and mirrored left tibiotarsus and fibula of *R. ostromi* (UA 8656) were originally created by O'Connor and Groenke and were downloaded from Morphosource. An existing mirrored left fibular mesh for *I. dispar* (FHSM 18702) was downloaded from Morphosource and supplemented with new meshes for the mirrored left femur and tibiotarsus (composite of a mirrored left proximal fragment and right distal fragment) of *I. dispar* (all YPM 1450) created from micro-CT scans (75–86 kV, 70–80 µA, 1-s exposure and 3,142 projections) and deposited in Morphosource. All Morphosource project IDs are provided in the Data availability statement.

Reporting summary

Further information on research design is available in the Nature Portfolio Reporting Summary linked to this article.

Data availability

Helmeted guineafowl and American alligator calibration images, X-ray videos and CT files for both in vivo and cadaveric studies have been deposited in the XMAPortal at http://xmaportal.org/webportal in collections titled 'Fibular Reduction' under study identifiers BROWN20, BROWN58 and BROWN71. Green iguana X-ray data have been deposited in the Jena Collection of X-ray Movies at https://szeb.thulb.uni-jena.de and are available on request as described by ref. 54. Meshes for *Marasuchus* are available on request from J. Hutchinson, and meshes for *Dinornis* are available on request from the Collections Manager of the Natural History Collections of the Canterbury Museum; both have been published[18]. Meshes and/or CT files for all other fossil specimens are available on Morphosource at https://www.morphosource.org/ (*Rahonavis* (project ID 00000C784); *Allosaurus*, *Deinonychus* and *Ichthyornis* (project ID 000638782; open download)). Extant avian meshes are available for download from Morphosource (*Poecile* (media ID 000093666; https://www.morphosource.org/concern/media/000093666?locale=en)) or the Idaho Museum of Natural History Virtualization Laboratory (all other taxa) at https://virtual.imnh.iri.isu.edu/. Source data are provided with this paper.

Code availability

The custom oRelFast.mel Maya embedded language script used to calculate joint kinematics in this study is available at https://bitbucket.org/xromm/xromm_other_mel_scripts/src/main/misc_utilities/. XMALab is pre-existing software previously described[52] and is available at https://bitbucket.org/xromm/xmaportal/src/master/, and the XROMM Maya Tools are pre-existing scripts available at https://bitbucket.org/xromm/xromm_mayatools/src/master/.

51. Tsai, H. P., Turner, M. L., Manafzadeh, A. R. & Gatesy, S. M. Contrast-enhanced XROMM reveals in vivo soft tissue interactions in the hip of *Alligator mississippiensis*. *J. Anat.* **236**, 288–304 (2020).
52. Knörlein, B. J., Baier, D. B., Gatesy, S. M., Laurence-Chasen, J. D. & Brainerd, E. L. Validation of XMALab software for marker-based XROMM. *J. Exp. Biol.* **219**, 3701–3711 (2016).
53. Turner, M. L. & Gatesy, S. M. Alligators employ intermetatarsal reconfiguration to modulate plantigrade ground contact. *J. Exp. Biol.* **224**, jeb242240 (2021).
54. Nyakatura, J. A. et al. Reverse-engineering the locomotion of a stem amniote. *Nature* **565**, 351–355 (2019).
55. Egawa, S. et al. The dinosaurian femoral head experienced a morphogenetic shift from torsion to growth along the avian stem. *Proc. R. Soc. B* **289**, 20220740 (2022).

Acknowledgements We thank D. Baier for developing and maintaining the XROMM Maya Tools; J. Hermanson, S. Nesbitt, T. Owerkowicz, K. Roorda, M. Stocker and R. Wilhite for providing cadaveric archosaur specimens; J. Hutchinson for providing *Marasuchus* meshes; M. Fox and V. Rhue for assistance with micro-CT scanning of and access to YPM specimens; V. Allen, P. Falkingham, R. Kambic, J. Lomax, T. Roberts, H. Tsai and M. Turner for assistance with X-ray data collection; and C. Gordon, C. Griffin, K. Jenkins, M. Margulis-Ohnuma, D. Meyer, K. Middleton, Z. Morris, J. Napoli, A. Ruebenstahl, M. J. Schwaner and A. Schulz for helpful discussion. A.R.M. and S.M.G. were supported by the Bushnell Research and Education Fund. A.R.M. was supported by a US NSF GRFP and PRFB (DBI-2209144), a Sigma Xi Grant-in-Aid of Research, a Society of Vertebrate Paleontology Cohen Award for Student Research, an Association of Women Geoscientists/Paleontological Society Winifred Goldring Award, a Brown University Presidential Fellowship, and a Yale Institute for Biospheric Studies Gaylord Donnelley Postdoctoral Environmental Fellowship. S.M.G. (grants IOS-0925077, DBI-0552051, IOS-0840950, DBI-1262156 and EAR-1452119) and B.-A.S.B. (CAREER (DEB-2046868)) were also supported by the US NSF. J.A.N. was supported by the Volkswagen Foundation (AZ 90222), the Daimler and Benz Foundation (32-08/12) and the German Research Council (DFG EXC 1027).

Author contributions A.R.M. and S.M.G. conceived the study and designed the experiments. A.R.M., S.M.G. and J.A.N. collected the X-ray data. A.R.M., S.M.G., J.A.N. and B.-A.S.B. collected the CT data. A.R.M. conducted the analyses and wrote the manuscript. All authors edited and approved the final manuscript.

Competing interests The authors declare no competing interests.

Additional information

Supplementary information The online version contains supplementary material available at https://doi.org/10.1038/s41586-024-08251-w.

Correspondence and requests for materials should be addressed to Armita R. Manafzadeh.

Peer review information *Nature* thanks Michael Benton, John Hutchinson and the other, anonymous, reviewer(s) for their contribution to the peer review of this work.

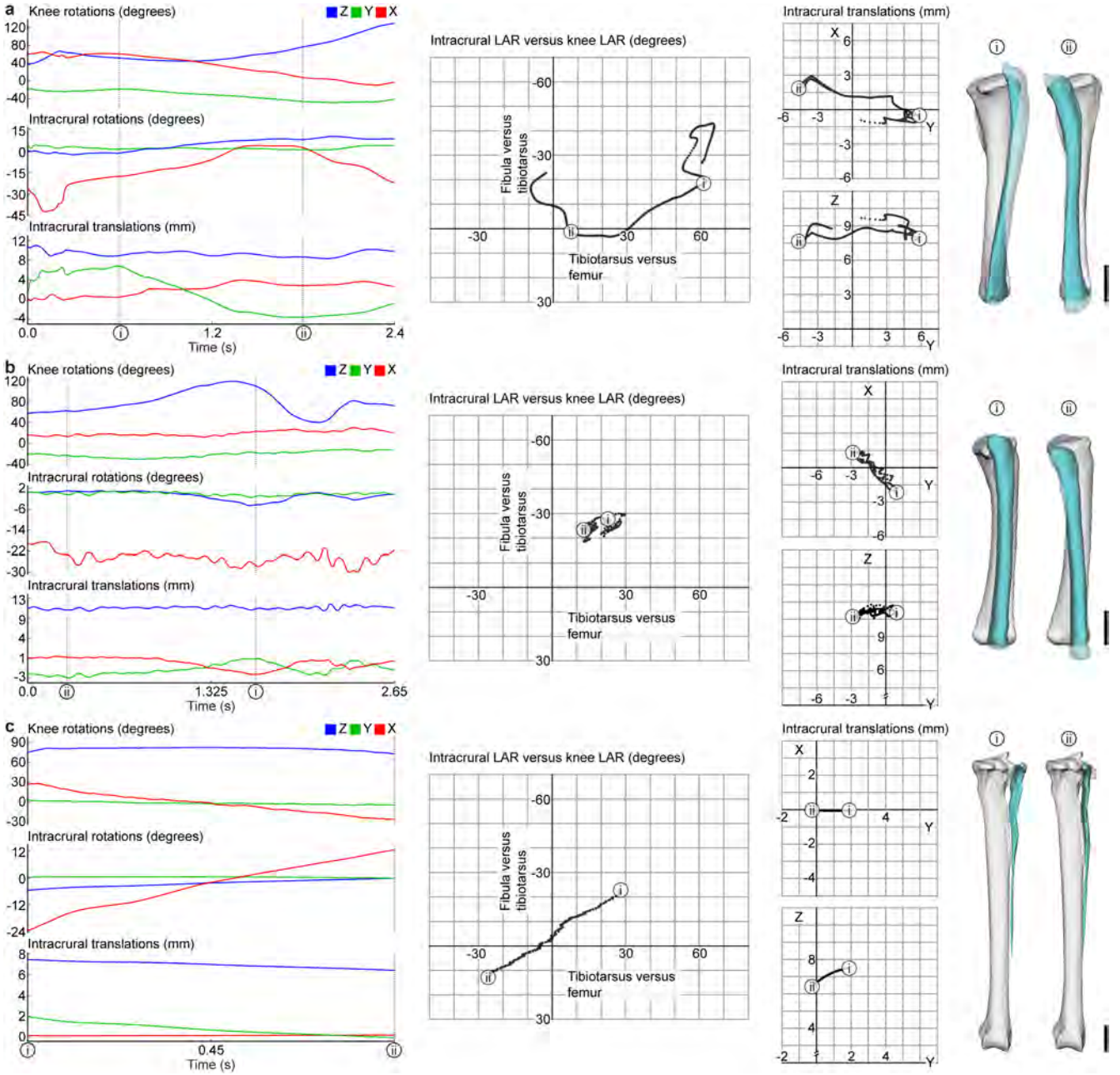

Extended Data Fig. 1 | In vivo intracrural kinematics in reptiles. XROMM-derived kinematics measured from *Iguana* (**a**), *Alligator* (**b**), and *Numida* (**c**) for the sequences displayed in Supplementary Videos 1–3. Representative crural poses reproduced from Fig. 2 are marked on each graph; note that *Alligator* configuration ii precedes configuration i, temporally. All scale bars for crura are 1 cm. Data were originally collected from left limbs in *Iguana* and *Numida* but have been mirrored to match right-handed sign conventions following ref. 18. Following ref. 18, at the knee, Z rotation corresponds to flexion-extension, extension is positive; Y rotation corresponds to abduction-adduction, adduction is positive; and X rotation corresponds to long-axis rotation, external rotation is positive. Within the crus, Z rotation corresponds to pitch, distal fibula rotating anteriorly is positive; Y rotation corresponds to yaw, distal fibula rotating medially is positive; X rotation corresponds to long-axis rotation or roll, external rotation is positive; Z translation is mediolateral, lateral motion of the fibula is positive; Y translation is anteroposterior, anterior motion of the fibula is positive; and X translation is proximodistal, distal motion of the fibula is positive. Note the flipped vertical axis in graphs displaying Knee LAR versus intracrural LAR. Video frames figured are n = 1200 for *Iguana*, n = 266 for *Alligator*, and n = 226 for *Numida*.

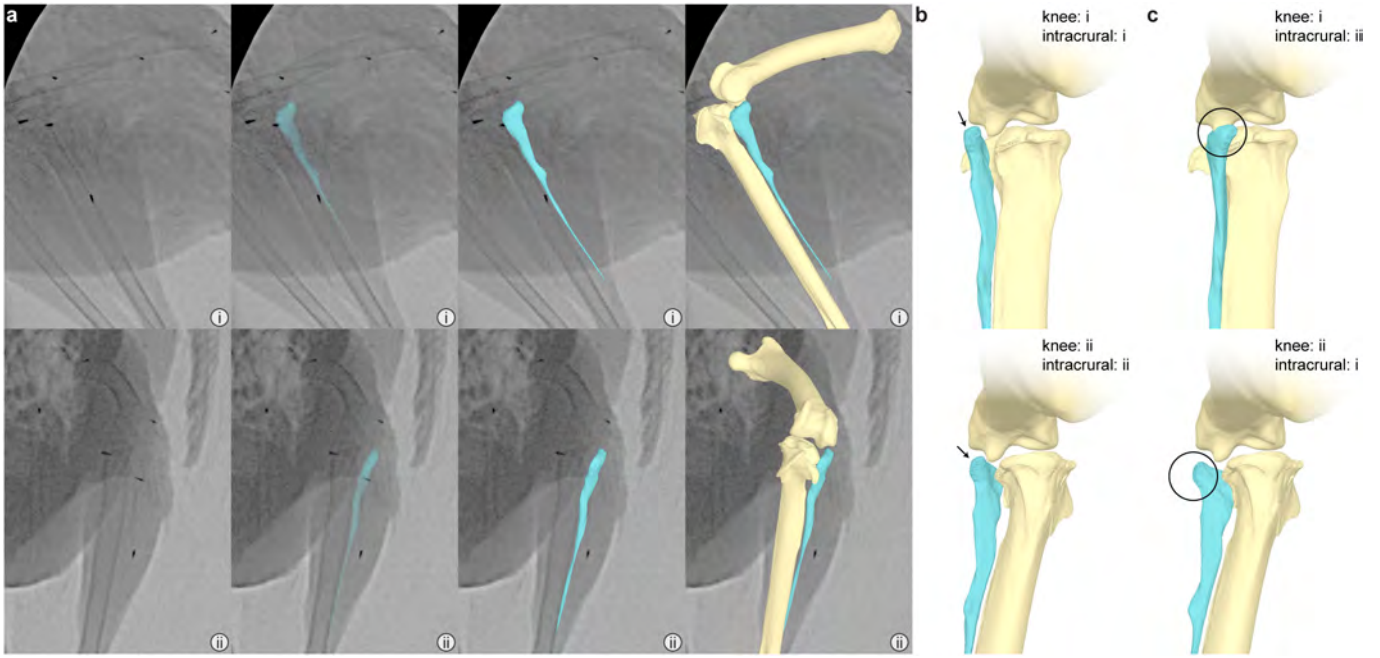

Extended Data Fig. 2 | X-ray Reconstruction of Moving Morphology evidence for avian intracrural motion. Scientific rotoscoping[14] requires alignment of mesh models to the shadows of bones in X-ray videos. During the guineafowl sequence displayed in Fig. 2, the proximal fibula is visible in X-ray videos as a faint shadow lateral to the larger elements of the knee. When the left fibular mesh is properly aligned to its shadow in two video frames (i and ii; **a**), the fibular head nestles within the femoral fibular trochlea (**b**; posterior view; proper articulation indicated with arrows). However, if the intracrural configurations from these two frames are swapped, the fibular head either interpenetrates with the lateral femoral condyle or disarticulates from the femur (**c**; posterior view; articular errors indicated with circles). Time points i and ii match those in Fig. 2 (i = t_1 and ii = t_3) and Extended Data Fig. 1.

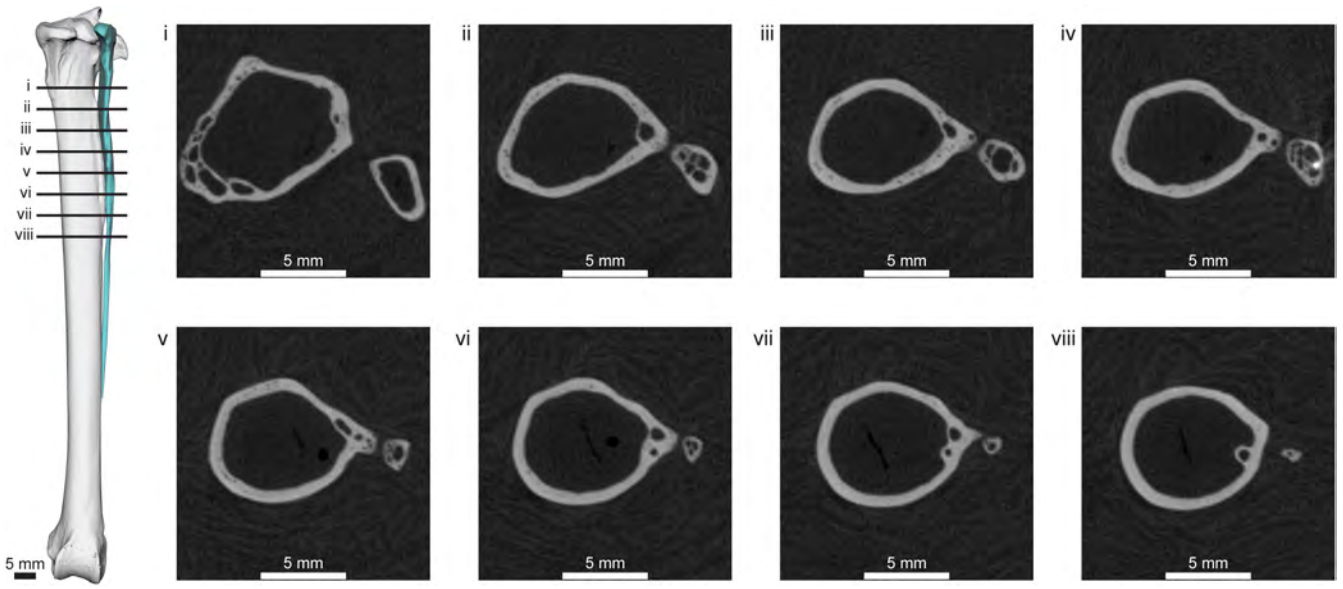

Extended Data Fig. 3 | Morphology of the avian intracrural articulation. Eight microcomputed tomography slices taken at five-millimetre intervals along a portion of a right helmeted guineafowl crus, demonstrating morphology of the articulation between the tibiotarsus (to the left in each slice) and the fibula (to the right in each slice). Slice positions are indicated on a 3-D model of the crus in posterior view, with the fibula coloured cyan as in Figs. 1, 2 and 4. The bright spot within the fibula in slice iv results from the presence of an implanted radiopaque marker for ex vivo XROMM analysis (see Methods).

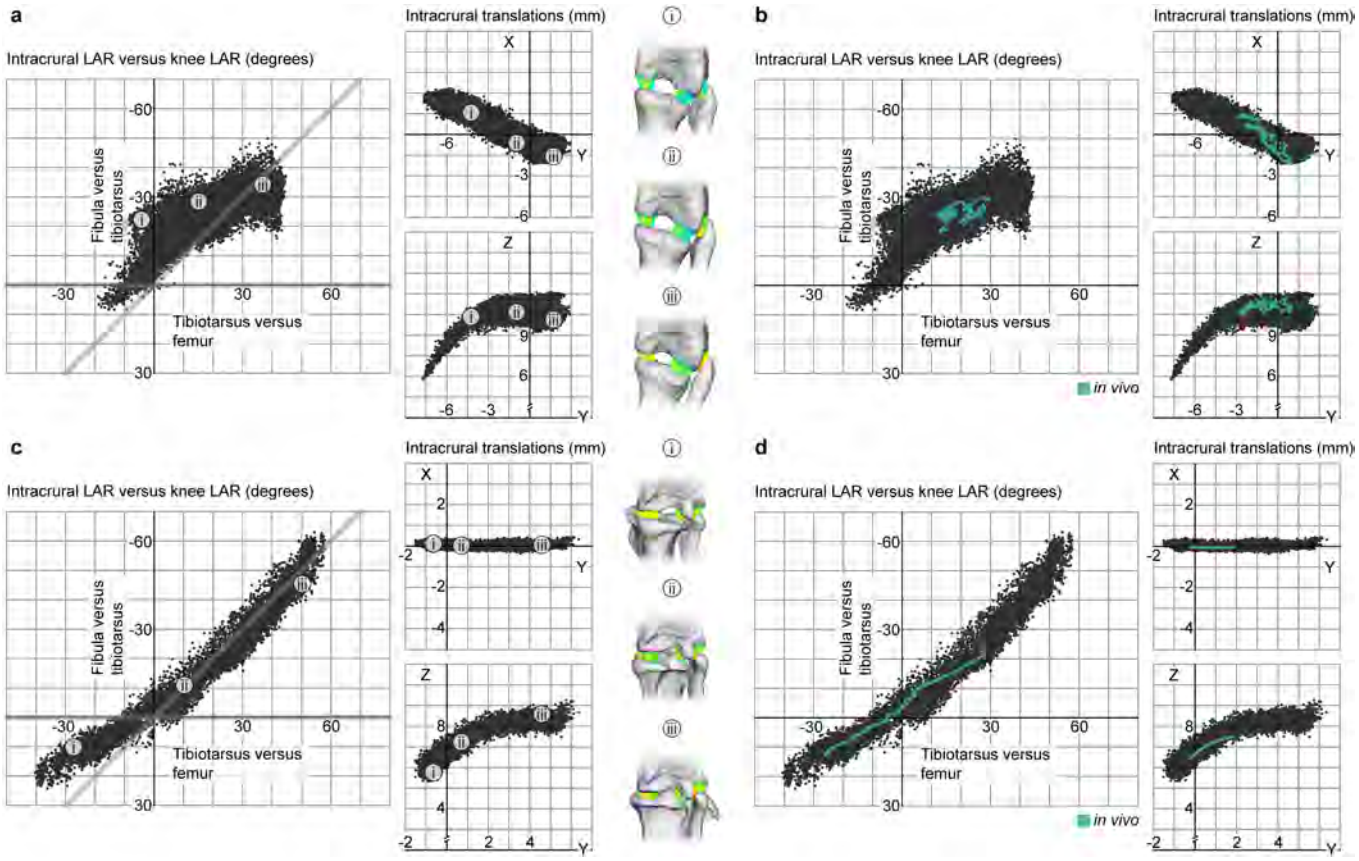

Extended Data Fig. 4 | Ex vivo intracrural kinematics in archosaurs. XROMM-derived kinematics measured from manipulations of *Alligator* (**a**), compared against in vivo data reproduced from Extended Data Fig. 1 (**b**), and from manipulations of *Numida* (**c**), compared against in vivo data reproduced from Extended Data Fig. 1 (**d**), display differences in intracrural mobility between species. In the lefthand column, points falling parallel to the horizontal axis (bolded) reflect the fibula axially rotating perfectly in concert with the tibiotarsus/tibia, with no measured intracrural LAR, whereas points paralleling the 1:1 line (bolded) reflect no axial rotation between the fibula and the femur. Note that in the bird, a much larger range of intracrural motion allows the fibula to stay tightly nestled within the femoral fibular trochlea (as indicated by proximity to the 1:1 line throughout), although this capacity weakens somewhat with internal rotation at the knee (left-hand portion of the graph). Note that in the alligator, a negative slope in the X-Y intracrural translation graph (compared to the negligible slope in the same graph for the bird) captures the skewing motion of the fibula visible in Fig. 2 and Supplementary Video 2. Representative knee poses corresponding to those in Fig. 3 are marked on each graph in **a** and **c**. Sign conventions match those in Extended Data Fig. 1. Video frames figured are n = 19,789 for *Alligator* and n = 10,723 for *Numida*.

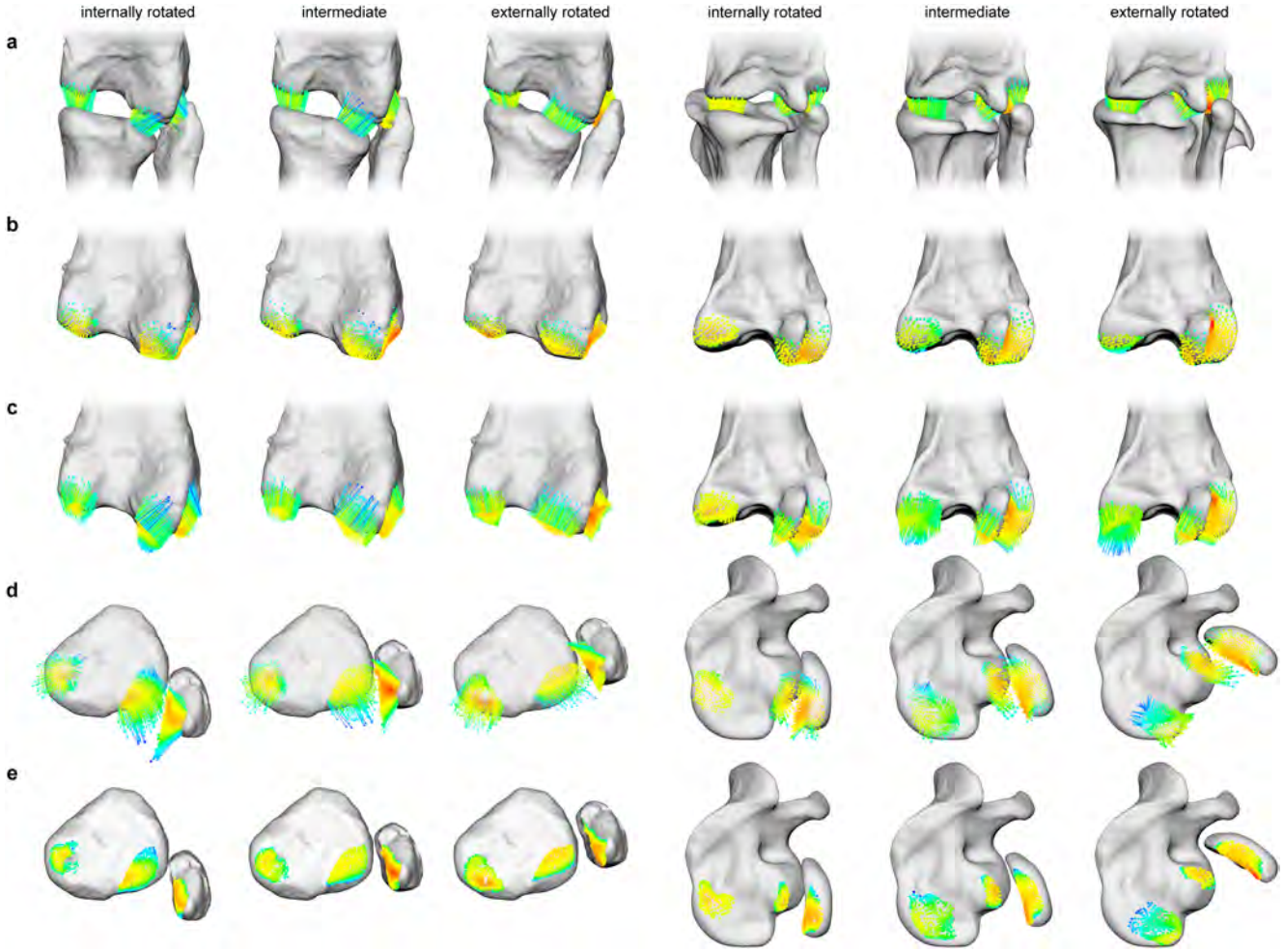

Extended Data Fig. 5 | Additional views of articular raycasts for archosaurian knee long-axis rotation. a, Articular raycasts in the alligator (left) and bird (right) right knee joints. Posterior view. **b**, Target points of the rays shown on isolated femora. Caudal view. **c**, Full rays shown on isolated femora. Caudal view. **d**, Full rays shown on isolated crura. Proximal view. **e**, Origin points of the rays shown on isolated crura. Proximal view. Rays coloured by length as in Fig. 3, throughout.

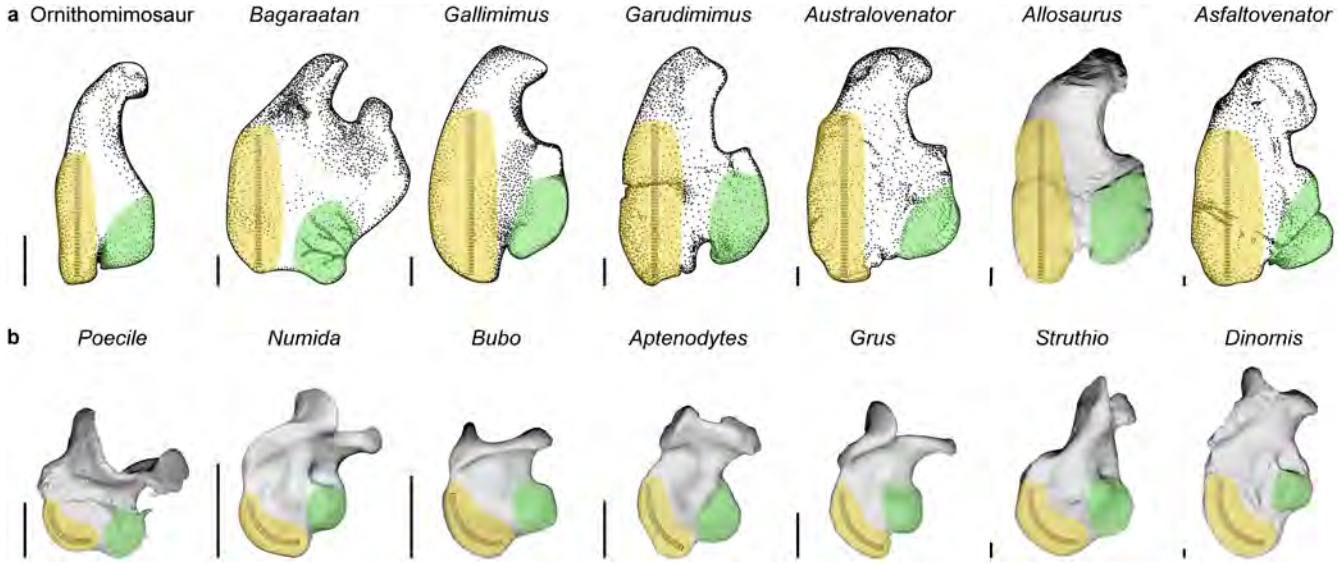

Extended Data Fig. 6 | Comparison of non-maniraptoran tetanuran and avian proximal tibias/tibiotarsi across body sizes. a, Homologous medial and lateral proximal surfaces coloured on non-maniraptoran tetanuran tibias demonstrate consistently roughly linear medial articular surfaces (yellow). Redrawn after literature figures; sources listed in Supplementary Information. **b**, Homologous medial and lateral proximal surfaces colored on avian tibiotarsi demonstrate consistently curved medial articular surfaces (yellow). All scale bars are 1 cm, except for *Poecile*, which is 1 mm. Differences in proximal medial surface curvature in these two groups yield a stark difference in the inferred capacity of the medial femoral condyle to travel along an arc-like path between rows, summarized by potential trajectories marked on each surface, following Figs. 3 and 4.

nature portfolio

Corresponding author(s): Armita R. Manafzadeh

Last updated by author(s): 10/11/2024

Reporting Summary

Nature Portfolio wishes to improve the reproducibility of the work that we publish. This form provides structure for consistency and transparency in reporting. For further information on Nature Portfolio policies, see our Editorial Policies and the Editorial Policy Checklist.

Statistics

For all statistical analyses, confirm that the following items are present in the figure legend, table legend, main text, or Methods section.

n/a	Confirmed
☐	☒ The exact sample size (*n*) for each experimental group/condition, given as a discrete number and unit of measurement
☒	☐ A statement on whether measurements were taken from distinct samples or whether the same sample was measured repeatedly
☒	☐ The statistical test(s) used AND whether they are one- or two-sided *Only common tests should be described solely by name; describe more complex techniques in the Methods section.*
☒	☐ A description of all covariates tested
☒	☐ A description of any assumptions or corrections, such as tests of normality and adjustment for multiple comparisons
☒	☐ A full description of the statistical parameters including central tendency (e.g. means) or other basic estimates (e.g. regression coefficient) AND variation (e.g. standard deviation) or associated estimates of uncertainty (e.g. confidence intervals)
☒	☐ For null hypothesis testing, the test statistic (e.g. *F*, *t*, *r*) with confidence intervals, effect sizes, degrees of freedom and *P* value noted *Give P values as exact values whenever suitable.*
☒	☐ For Bayesian analysis, information on the choice of priors and Markov chain Monte Carlo settings
☒	☐ For hierarchical and complex designs, identification of the appropriate level for tests and full reporting of outcomes
☒	☐ Estimates of effect sizes (e.g. Cohen's *d*, Pearson's *r*), indicating how they were calculated

Our web collection on statistics for biologists contains articles on many of the points above.

Software and code

Policy information about availability of computer code

Data collection	Native functions within XMALab Version 2.1.0 and Autodesk Maya versions 2020-2025 were used to collect data (no custom code).
Data analysis	The custom oRelFast.mel Maya Embedded Language Script used to calculate joint kinematics in this study is available at https://bitbucket.org/xromm/xromm_other_mel_scripts/src/main/misc_utilities/. XMALab is pre-existing software described by ref.51 and is available at https://bitbucket.org/xromm/xmaportal/src/master/ and the XROMM Maya Tools are pre-existing scripts available at https://bitbucket.org/xromm/xromm_mayatools/src/master/. Native functions within Maya 2025 were used to plot data.

For manuscripts utilizing custom algorithms or software that are central to the research but not yet described in published literature, software must be made available to editors and reviewers. We strongly encourage code deposition in a community repository (e.g. GitHub). See the Nature Portfolio guidelines for submitting code & software for further information.

Data

Policy information about availability of data

All manuscripts must include a data availability statement. This statement should provide the following information, where applicable:

- Accession codes, unique identifiers, or web links for publicly available datasets
- A description of any restrictions on data availability
- For clinical datasets or third party data, please ensure that the statement adheres to our policy

Helmeted Guineafowl and American alligator calibration images, X-ray videos, and computed tomography files for both in vivo and cadaveric studies are deposited

in the XMAPortal at http://xmaportal.org/webportal in collections titled 'Fibular Reduction' under study identifiers BROWN20 (https://xmaportal.org/webportal/larequest.php?request=CollectionView&StudyID=20&instit=BROWN&collectionID=29), BROWN58 (https://xmaportal.org/webportal/larequest.php?request=CollectionView&StudyID=58&instit=BROWN&collectionID=30), and BROWN71 (https://xmaportal.org/webportal/larequest.php?request=CollectionView&StudyID=71&instit=BROWN&collectionID=31) . Green iguana X-ray data are deposited in the Jena Collection of X-ray Movies at https://szeb.thulb.uni-jena.de and are available on request as described by ref.54. Meshes for Marasuchus are available on request from J. Hutchinson and meshes for Dinornis are available on request from the Collections Manager of the Natural History Collections of the Canterbury Museum; both were initially published by ref.18. Meshes and/or computed tomography files for all other fossil specimens are available on Morphosource at https://www.morphosource.org/ (Rahonavis [Project ID: 00000C784; https://www.morphosource.org/projects/00000C784]; Allosaurus, Deinonychus, and Ichthyornis [Project ID: 000638782; open download; https://www.morphosource.org/projects/000638782])). Extant avian meshes are available for download from Morphosource (Poecile [Specimen ID: 000S26550]) or the Idaho Museum of Natural History Virtualization Laboratory (all other taxa) at https://virtual.imnh.iri.isu.edu/.

Research involving human participants, their data, or biological material

Policy information about studies with human participants or human data. See also policy information about sex, gender (identity/presentation), and sexual orientation and race, ethnicity and racism.

Reporting on sex and gender	N/A
Reporting on race, ethnicity, or other socially relevant groupings	N/A
Population characteristics	N/A
Recruitment	N/A
Ethics oversight	N/A

Note that full information on the approval of the study protocol must also be provided in the manuscript.

Field-specific reporting

Please select the one below that is the best fit for your research. If you are not sure, read the appropriate sections before making your selection.

☒ Life sciences ☐ Behavioural & social sciences ☐ Ecological, evolutionary & environmental sciences

For a reference copy of the document with all sections, see nature.com/documents/nr-reporting-summary-flat.pdf

Life sciences study design

All studies must disclose on these points even when the disclosure is negative.

Sample size	Existing in vivo hindlimb skeletal motion datasets (Kambic et al., 2014; Manafzadeh et al., 2021; Tsai et al., 2020; Nyakatura et al., 2019) were reanalyzed. One hindlimb from each of two cadaveric birds, and three hindlimbs total from two cadaveric alligators, were analyzed, as were one sequence of in vivo data from each taxon (bird, alligator, iguana). In vivo analysis was exploratory in nature, requiring only one sequence of data per animal, resulting in n = 1200 video frames for Iguana, n = 266 video frames for Alligator, and n = 226 video frames for Numida. Cadaveric sample sizes were deemed sufficient to capture joint mobility based on previous mobility analyses of the same individuals (Manafzadeh et al. 2021 PNAS), resulting in n = 10800 video frames analyzed for Numida and n = 19800 video frames analyzed for Alligator.
Data exclusions	In 77 frames of Numida video, fibular markers were insufficiently visible to facilitate reliable tracking and these frames were excluded from analysis. In 11 frames of Alligator video the fibula was out of view and these frames were excluded from analysis.
Replication	N/A; this study did not involve experimental groups, all cadaveric mobility data were pooled on a per-taxon basis as previously described by Manafzadeh et al. 2021 (PNAS) to ensure complete coverage of joint mobility.
Randomization	N/A; this study did not involve experimental groups.
Blinding	N/A; this study did not involve experimental groups.

Reporting for specific materials, systems and methods

We require information from authors about some types of materials, experimental systems and methods used in many studies. Here, indicate whether each material, system or method listed is relevant to your study. If you are not sure if a list item applies to your research, read the appropriate section before selecting a response.

Materials & experimental systems

n/a	Involved in the study
☒	☐ Antibodies
☒	☐ Eukaryotic cell lines
☐	☒ Palaeontology and archaeology
☐	☒ Animals and other organisms
☒	☐ Clinical data
☒	☐ Dual use research of concern
☒	☐ Plants

Methods

n/a	Involved in the study
☒	☐ ChIP-seq
☒	☐ Flow cytometry
☒	☐ MRI-based neuroimaging

Palaeontology and Archaeology

Specimen provenance	N/A; the specimens used in this study are existing specimens and casts housed at the Yale Peabody Museum.
Specimen deposition	The specimens used in this study are existing specimens and casts housed at the Yale Peabody Museum.
Dating methods	N/A; the specimens used in this study are existing specimens and casts housed at the Yale Peabody Museum.5205.

☐ Tick this box to confirm that the raw and calibrated dates are available in the paper or in Supplementary Information.

Ethics oversight	N/A

Note that full information on the approval of the study protocol must also be provided in the manuscript.

Animals and other research organisms

Policy information about studies involving animals; ARRIVE guidelines recommended for reporting animal research, and Sex and Gender in Research

Laboratory animals	All reptile in vivo data reported here was originally reported by Kambic et al., 2014; Manafzadeh et al., 2021; Tsai et al., 2020; Nyakatura et al., 2019; see those publications for full information.
Wild animals	N/A
Reporting on sex	N/A
Field-collected samples	N/A
Ethics oversight	All procedures involving live animals were approved by the Brown University Institutional Animal Care and Use Committee or the responsible authorities in Thuringia, Germany (Thüringer Landesamt für Verbraucher- und Umweltschutz).

Note that full information on the approval of the study protocol must also be provided in the manuscript.